frontiers | Frontiers in Energy Research

TYPE Original Research
PUBLISHED 28 September 2022
DOI 10.3389/fenrg.2022.966975

OPEN ACCESS

EDITED BY
Dongran Song,
Central South University, China

REVIEWED BY
Jian Yang,
Central South University, China
Rizk Masoud,
University of Menoufia, Egypt

*CORRESPONDENCE
Elmazeg Elgamli,
Elgamlies@cardiff.ac.uk

SPECIALTY SECTION
This article was submitted to Smart Grids,
a section of the journal
Frontiers in Energy Research

RECEIVED 12 June 2022
ACCEPTED 12 July 2022
PUBLISHED 28 September 2022

CITATION
Jaiswal A, Belkhier Y, Chandra S, Priyadarshi A, Bajaj M, Pushkarna M, Elgamli E, Shouran M and Kamel S (2022), Design and implementation of energy reshaping based fuzzy logic control for optimal power extraction of PMSG wind energy converter.
Front. Energy Res. 10:966975.
doi: 10.3389/fenrg.2022.966975

Design and implementation of energy reshaping based fuzzy logic control for optimal power extraction of PMSG wind energy converter

Ashish Jaiswal[1], Youcef Belkhier[2], Subhash Chandra[1], Anurag Priyadarshi[1], Mohit Bajaj[3], Mukesh Pushkarna[1], Elmazeg Elgamli[4]*, Mokhtar Shouran[4] and Salah Kamel[5]

[1]Department of Electrical Engineering, GLA University Mathura, Mathura, India, [2]Centre for Ocean Energy Research, Maynooth University, Maynooth, Kildare, [3]Department of Electrical Engineering, Graphic Era (Deemed to be University), Dehradun, India, [4]Wolfson Centre for Magnetics, School of Engineering, Cardiff University, Cardiff, United Kingdom, [5]Department of Electrical Engineering, Faculty of Engineering, Aswan University, Aswan, Egypt

Given the greater penetration of wind power, the impact of wind generators on grid electricity reliability imposes additional requirements. One of the most common technologies in wind power generating schemes is the permanent magnet synchronous generator (PMSG) converter. However, the controller calculation is difficult due to the nonlinear dynamical and time-varying characteristics of this type of conversion system. This study develops a unique intelligent controller approach based on the passivity notion that tracks velocity and maintains it functioning at the optimum torque. To address the robustness issues encountered by traditional generator-side converter (MSC) strategies such as proportional-integral (PI), this suggested scheme integrates a passivity-based procedure with a fuzzy logic control (FLC) methodology for a PMSG-based wind power converter. The suggested controller is distinguished by the fact that the nonlinear features are compensated in a damped manner rather than canceled. To achieve the required dynamic, the fuzzy controller is used, which ensures quick convergence and global stability of the closed loop system. The development of the maximum power collected, the lowered fixed gains, and the real-time application of the control method are the primary contributions and novelties. The primary objectives of this project are to manage DC voltage and attain adequate reactive power levels in order to provide dependable and efficient electricity to the grid. The proposed scheme is being used to regulate the MSC, while the grid-side employs a traditional proportional-integral method. The efficiency of the suggested technique is investigated numerically using MATLAB/Simulink software. Furthermore, the processor-in-the-loop (PIL) tests are carried out to demonstrate that the suggested regulator is practically implementable.

KEYWORDS

renewable energy systems, fuzzy logic control, processor-in-the loop (PIL) experiments, nonlinear control, power extraction

Introduction

Sustainable energy source innovations are turning into an expanding option to address the issues of environmental change. One of the most promising types of renewable energy is wind energy. Wind power has been in full industrial growth for some years. Indeed, it has several advantages: first and foremost, it is a non-polluting renewable energy source that helps to improve air quality and the reduction of greenhouse gas emissions. It is also a form of energy that makes use of domestic resources and so helps to energy independence and supply security, its high-power density, and a high potential for electricity generation (Soliman et al., 2021). The role of a wind turbine is to convert the kinetic energy of the wind into electrical energy. Its various elements are designed to maximize this energy conversion. There are several technologies that are used to capture the energy of the wind (vertical axis or horizontal axis), and also, different configurations of a wind turbine system (fixed speed and variable speed). Therefore, wind turbines are considered with variable power generators, connected to the electrical grid. The amount of energy recovered by variable speed wind energy conversion systems (VS-WECS) depends on the accuracy of the maximum power point tracking (MPPT) search and also on the type of generator used. The associated power conversion chains often use a PMSG (Soliman et al., 2021), (Mohammadi et al., 2019). This type of machine allows making it possible to get rid of the problem of the excitation current supply, which is difficult to manage in a conventional synchronous machine (Mohammadi et al., 2019). However, due to unknown modeling inaccuracy, dynamic characteristics, and non-linearities, control system computation for the PMSG remains a difficult task (Wang and Wang, 2020). In the literature, there has been several research studies related to the nonlinear control of PMSG. In the study by Saidi et al. (2019), a tip-speed ratio technique associated with an integral backstepping controller is suggested. A mechanical sensorless control strategy-based nonlinear observer is proposed (Fantino et al., 2016). In the work of Zargham and Mazinan (2019), a super-twisting sliding mode controller is designed. A new direct torque of a fault-tolerant direct-driven PMSG controller is developed (Jlassi and Cardoso, 2019). To achieve direct power control, an optimal voltage vector-based modulated model predictive control is developed in Bigarelli et al. (2020). Further, in the study by Haq et al. (2020), a maximum power extraction-based feed-forward neural network and generalized global sliding mode controller are investigated. Meanwhile, an autonomous PMSG-based wind conversion system is controlled by using a cascade neural networks algorithm (Chandrasekaran et al., 2020). More recently, a nonlinear model predictive control with the fuzzy regulator is proposed in Song et al. (2022a), for the optimization of the energy capture and torque fluctuation of wind turbines. In the study by Song et al. (2022b), a stochastic model predictive yaw control strategy based on intelligent scenario generation is proposed to improve the energy capture efficiency of wind energy converters. A chaos-opposition-enhanced slime mould algorithm to minimize energy cost for the wind turbines on high-altitude sites is developed in Rizk-Allah et al. (2022), the proposed model is established based on rotor radius, rated power, and hub height needed to achieve an optimal design model. However, as stated in Yang et al. (2013), most of such controls are dependent on signals and therefore do not consider the structural properties of the PMSG when building the regulator.

The present article investigates a new control approach based on the passivity notion, a new fuzzy passivity-based control (PBC) to design an optimal controller for the PMSG, which tracks speed and maintains it functioning at the optimal torque. Inherent advantages of the PBC method are that the nonlinear terms are adjusted in a damped manner rather than being eliminated that the assured stability, as well as the promised robustness qualities (Nicklasson et al., 1994), (Belkhier et al., 2022). The study's major goal is to highlight a hybrid control method for VS-WECS, to enable efficient power integration to the grid and increase the PMSG operational speed.

Several techniques have been reported in the literature based on the passivity control method to improve the performance of the PMSG and increase the efficiency of wind energy conversion systems. A sliding mode strategy (SMC) associated with PBC is adopted in Yang et al. (2018a). However, as the authors point out, the provided coupled PBC-SMC controlling employs over six fixed gains, making it hard to find their ideal settings. A passivity-based linear feedback current control approach is developed for a PMSG in Belkhier and Achour (2020a), where the authors proposed PBC with an orientation of the flux, where the desired current is computed by a PI controller. However, the use of the PI implies fixed gains, which brings a significant sensitivity to disturbances that can affect the functioning of the system. In Subramaniam and Joo (2019), a PBC-SMC and fuzzy controller is proposed. However, the suggested combined strategy's controller design is complex due to mathematical constraints; passivity-based linear feedback control is explored in Yang et al. (2018b). However, nonlinear properties and the robustness due to parameter changes of the PMSG have not been evaluated. In Belkhier and Achour (2020b), a passivity-based backstepping is proposed. However, due to mathematical limitations, the controller design of the proposed combination method is complicated.

As it was mentioned before, several aspects were neglected by the works carried out. In order to make more improvements and

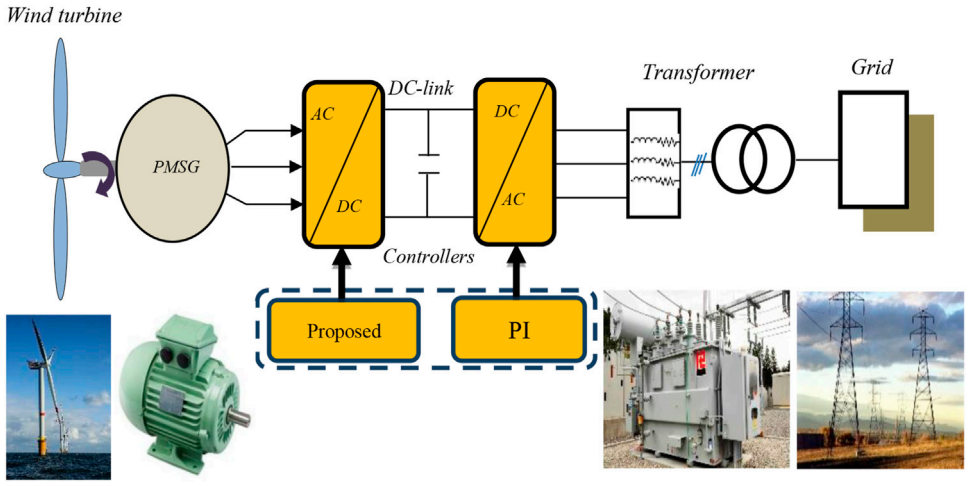

FIGURE 1
Wind power system.

contributions to what was performed. The present work is split into two sections. First, a fuzzy-PBC system is used to ensure that the PMSG receives continuous power from the wind source, increase the PMSG operational speed, and rectify non-linearities, external disturbances, and parametric fluctuations in the PMSG. The second is devoted to applying the classical PI control to regulating the grid-side power and voltage. A special focus is given to the control of the PMSG, by synthesizing the new suggested control scheme while considering the complete dynamic of the PMSG. In addition, the resilience over parameter variations has received considerable consideration. Also, experimental testing of the investigated strategy is conducted using a DSP card, and the results show clearly that the present system is applicable practically.

The contribution and novelty of the present article are summarized as follows:

- A novel control technique based on hybrid fuzzy-PBC for optimum efficiency of the PMSG is presented to ensure a quick convergence of the locked system and energy extraction.
- By simulating the unstructured dynamics of the PMSG, the fuzzy manager is employed for gain adjustment, which meets the requirements produced by incorrect variables to calculate the appropriate dynamics and considerably enhances the resilience of the system.
- Numerous numerical studies are conducted to show how resilient the suggested technique is to parameter changes and outside disruptions. In addition, analytical proof of the closed-stability loop's and exponential convergence has been provided.
- The novelty of the proposed control lies in its structure, which is really very simple and contains only one fixed gain, which is the damping gain of the control, which makes it particularly robust and increases resilience and global stability, as demonstrated in the results section.
- Experimental validation of the proposed control schemes is conducted using processor-in-the loop (PIL) and the results show clearly that the present system is applicable practically.

The current article is arranged in the following manner: *Introduction* establishes the system description. The proposed strategy calculation is discussed in *Introduction*. Concerning *Introduction*, grid-side converter (GSC) voltage and management is presented. In *Introduction*, simulation experimental results are exposed. Finally, *Introduction* finishes with the main findings and recommendations for future research.

System description

Figure 1 shows the setup of the MATLAB/Simulink-based wind energy converter, which includes a wind turbine, PMSG, AC-DC-AC converter, and main electrical network.

Wind power

The wind energy converter model is represented as follows (Fantino et al., 2016; Belkhier et al., 2020):

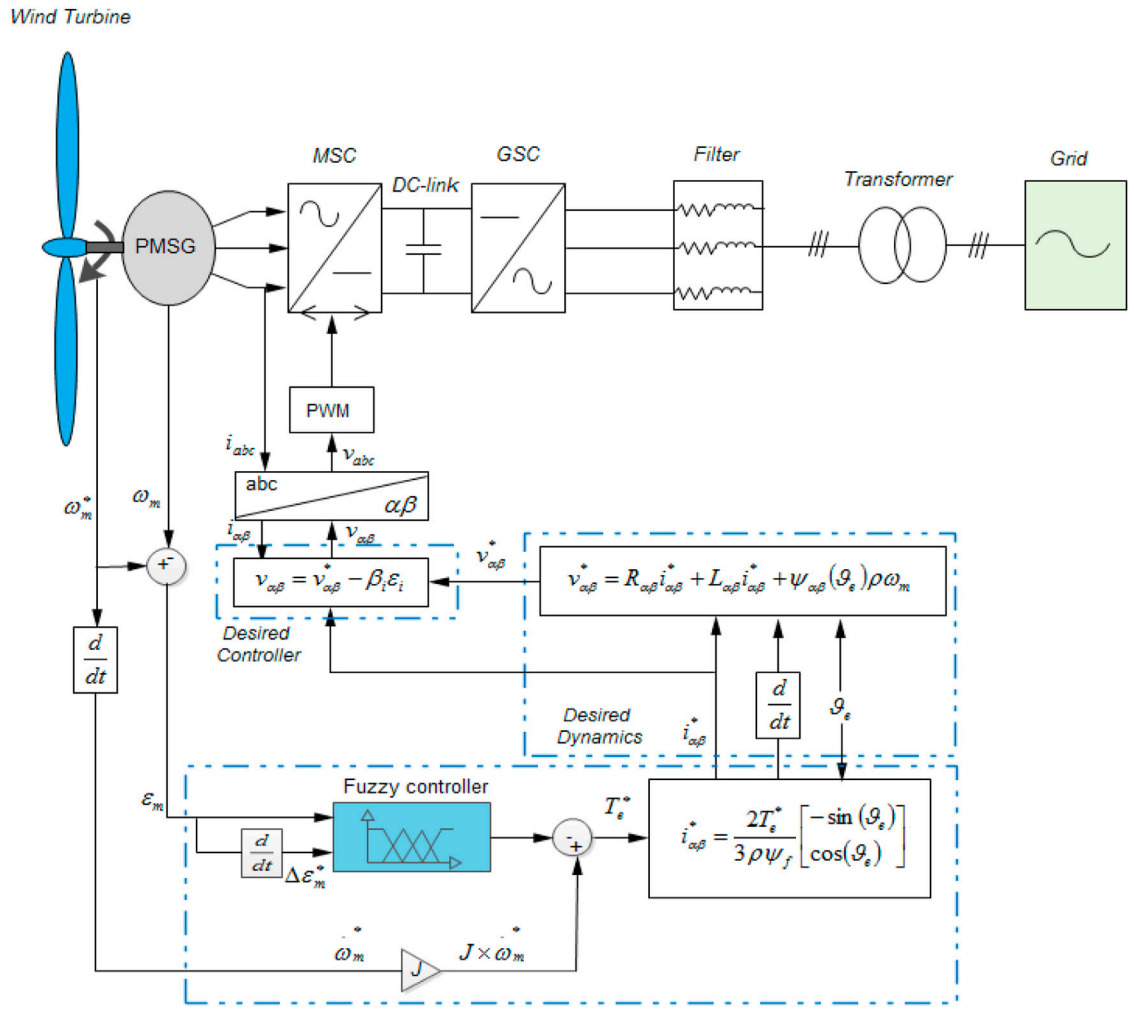

FIGURE 2
Schematic of the proposed controller.

$$P_m = \frac{1}{2}\rho C_p(\beta,\lambda)Av_s^3, \tag{1}$$

$$T_m = \frac{P_m}{\omega_t}, \tag{2}$$

$$C_p(\beta,\lambda) = 0.5\left(\frac{116}{\lambda_i} - 0.4\beta - 5\right)e^{-\left(\frac{21}{\lambda_i}\right)}, \tag{3}$$

$$\lambda_i^{-1} = (\lambda + 0.08\beta)^{-1} - 0.035(1+\beta^3)^{-1}, \tag{4}$$

$$\lambda = \frac{\omega_t R}{v_s}, \tag{5}$$

where P_m depicts the wind power captured, T_m is the wind turbine output torque, A depicts the blades' area, ρ is fluid density, λ is speed ratio, v_s denotes the wind speed, β depicts pitch angle, ω_t depicts turbine speed, R is the blades' radius, and C_p is power coefficient.

Permanent magnet synchronous generator modeling

The PMSG modeling according to αβ-frame is needed to design the proposed technique, which is formulated as (Soliman et al., 2021; Belkhier et al., 2022):

$$L_{\alpha\beta}\frac{di_{\alpha\beta}}{dt} + \psi_{\alpha\beta}(\theta_e)p\omega_m = v_{\alpha\beta} - R_{\alpha\beta}i_{\alpha\beta}, \tag{6}$$

$$C\frac{d\omega_m}{dt} = T_m - T_e\left(i_{\alpha\beta},\theta_e\right) - f_{fv}\omega_m, \tag{7}$$

$$T_e\left(i_{\alpha\beta},\theta_e\right) = \psi_{\alpha\beta}^T(\theta_e)i_{\alpha\beta}, \tag{8}$$

where p denotes the pair pole numbers, J represents the moment of the inertia, $i_{\alpha\beta} = \begin{bmatrix} i_\alpha \\ i_\beta \end{bmatrix}$ indicates the current, T_e indicates electromagnetic torque, $L_{\alpha\beta} = \begin{bmatrix} L_\alpha & 0 \\ 0 & L_\beta \end{bmatrix}$ indicates induction's

stator, f_{fv} indicates viscosity parameter, θ_e indicates electrical angular, $v_{\alpha\beta} = \begin{bmatrix} v_\alpha \\ v_\beta \end{bmatrix}$ indicates stator's voltage, $R_{\alpha\beta} = \begin{bmatrix} R_S & 0 \\ 0 & R_s \end{bmatrix}$ indicates the resistance, $\psi_{\alpha\beta}(\theta_e) = \psi_f \begin{bmatrix} -\sin(\theta_e) \\ \cos(\theta_e) \end{bmatrix}$ indicates linkages' flux, and ω_m indicates motor speed.

Proposed controller computation

Several stages must be validated in order to build the developed technique: at first, the passivity attribute of the PMSG model must be demonstrated so that the suggested approach may be used. Second, the PMSG must be broken down into two passive subsystems with negative feedback. Finally, in order to construct a controller with a simple structure, the non-dissipative variables in the PMSG model must be formulated. Figure 2 depicts the explored strategy computing process, which has two distinct components: the first phase consists in designing the reference current using the computed electromagnetic torque and the high order sliding mode control (HSMC) technique, and the needed current is subsequently calculated using the required torque. In the second portion, the controller law is computed using the created method-based HSMC.

PMSG αβ-model interconnected subsystems decomposition

From Eq. 6, the following relationship is formulated:

$$\sum_e : V_e = \begin{bmatrix} v_{\alpha\beta} \\ -\omega_m \end{bmatrix} \rightarrow Y_e = \begin{bmatrix} i_{\alpha\beta} \\ T_m \end{bmatrix}. \tag{9}$$

From Eqs 7, 8, the following relationship is formulated:

$$\sum_m : V_m = (-T_e + T_m) \rightarrow Y_e = -\omega_m = \frac{(-T_e + T_m)}{Js + f_{fv}}. \tag{10}$$

According to (9) and (10) the upcoming lemma is yield:

Lemma 1: *according to the aforementioned conditions, the PMSG in the dq-model can be decomposed into feedback interconnected two passive subsystems, electrical subsystem* $\sum_e$ *and mechanical subsystem* $\sum_m$.

Proof: from (9), the following PMSG total energy H_e is given as:

$$H_e = \frac{1}{2} i_{\alpha\beta}^T L_{\alpha\beta} i_{\alpha\beta} + \psi_{\alpha\beta}^T i_{\alpha\beta}. \tag{11}$$

The time derivative of H_e along (6), yields:

$$\dot{H}_e = -i_{\alpha\beta}^T R_{\alpha\beta} i_{\alpha\beta} + Y_e^T V_e + \frac{d}{dt}\left(\psi_{\alpha\beta}^T i_{\alpha\beta}\right). \tag{12}$$

Integrating on both sides of (12) along $[0 \quad T_e]$, gives:

$$\underbrace{H_e(T_e) - H_e(0)}_{Stored\ Energy} = -\underbrace{\int_0^{T_e} i_{\alpha\beta}^T R_{\alpha\beta} i_{\alpha\beta} d\tau}_{Dissipated\ Energy} + \underbrace{\int_0^{T_e} Y_e^T V_e d\tau + \left[\psi_{\alpha\beta}^T i_{\alpha\beta}\right]_0^{T_e}}_{Supplied\ Energy}. \tag{13}$$

Here, $H_e(T_e) \geq 0$ and $H_e(0)$ indicate stored energy initially. By Increasing Eq. 13, the following inequality dissipation is formulated:

$$\int_0^{T_e} Y_e^T V_e d\tau \geq \lambda_{min}\{R_{\alpha\beta}\} \int_0^{T_e} \|i_{\alpha\beta}\|^2 d\tau - \left(H_e(0) + \left[\psi_{\alpha\beta}^T i_{\alpha\beta}\right]_0^{T_e}\right), \tag{14}$$

where $\|.\|$ indicates Euclidian norm's vector.

It is clearly indicated that $\sum_e$ is passive. Then, from $\sum_m$, the transfer function $F_m(s)$ is deduced and formulated as:

$$\mathrm{F}_m(s) = \frac{\mathrm{Y}_m(s)}{\mathrm{V}_m(s)} = \frac{1}{\mathrm{J}s + f_{fv}}. \tag{15}$$

It can be deduced that $\sum_m$ is passive, since $\mathbf{F}_m(s)$ is strictly positive. Thus, the PMSG model is decomposable into two passive subsystems.

PMSG passivity property

Lemma 2: *the model (6)–(8) is passive, when* $Y = [v_{\alpha\beta}^T, T_e]^T$ *and* $X = [i_{\alpha\beta}^T, \omega_m]^T$ *are chosen as the PMSG outputs and inputs,* respectively.

Proof: first, the PMSG Hamiltonian H_m is defined as:

$$H_m\left(i_{\alpha\beta}, \omega_m\right) = \underbrace{\frac{1}{2} i_{\alpha\beta}^T L_{\alpha\beta} i_{\alpha\beta} + \frac{1}{2} i_{\alpha\beta}^T L_{\alpha\beta} i_{\alpha\beta}}_{Electrical\ Energy} + \underbrace{\frac{1}{2} J\omega_m^2}_{Mecanical\ Energy}. \tag{16}$$

Derivative along (6)–8) of H_m, gives:

$$\frac{dH_m\left(i_{\alpha\beta}, \omega_m\right)}{dt} = -\frac{d\left(i_{\alpha\beta}^T R\, i_{dq}\right)}{dt} + y^T v + \frac{d}{dt}\left(\psi_{\alpha\beta}^T i_{\alpha\beta}\right), \tag{17}$$

where $R = \mathrm{diag}\{R_{\alpha\beta}, f_{fv}\}$. Integrating (17) along $[0 \ T_m]$, gives:

$$\underbrace{H_m(T_m) - H_m(0)}_{Stored\ Energy} = -\underbrace{\int_0^{T_m} i_{\alpha\beta}^T R\, i_{\alpha\beta}\, d\tau}_{Dissipated\ Energy} + \underbrace{\int_0^{T_m} y^T v\, d\tau + \left[\psi_{\alpha\beta}^T i_{\alpha\beta}\right]_0^{T_m}}_{Supplied\ Energy}, \tag{18}$$

where $H_m(0)$ is the stored initial energy and $H_m(T_m) \geq 0$. Integrating (18) yields:

$$\int_0^{T_m} y^T v\, d\tau \geq \lambda_{\min}\{R\} \int_0^{T_m} \|i_{\alpha\beta}\|^2 d\tau - \left(H_m(0) + \left[\psi_{\alpha\beta}^T i_{\alpha\beta}\right]_0^{T_m}\right). \tag{19}$$

Then, relationship M is passive, which is the same for the PMSG.

Controller law design process

According to the model (6)–(8), one can formulate the reference dynamics given as follows:

$$v^*_{\alpha\beta} = L_{\alpha\beta}\frac{di^*_{\alpha\beta}}{dt} + \psi_{\alpha\beta}(\theta_e)p\omega_m + R_{\alpha\beta}i^*_{\alpha\beta}, \tag{20}$$

$$T_m = J\frac{d\omega^*_m}{dt} - T^*_e\left(i^*_{\alpha\beta}, \theta_e\right) - f_{fv}\omega^*_m, \tag{21}$$

where $i^*_{\alpha\beta}$ represents the reference current, $v^*_{\alpha\beta}$ represents the reference voltage, ω^*_m denotes speed of the turbine, and T^*_e denotes the reference torque. To ensure zero error convergence of between the reference and the measured dynamics, it is aimed to compute $v_{\alpha\beta}$. Thus, the error between the desired model (20)–(21) and the measured model (6)–(8) is formulated as:

$$v_{\alpha\beta} - v^*_{\alpha\beta} = L_{\alpha\beta}\frac{d\varepsilon_i}{dt} + R_{\alpha\beta}\left(i^*_{\alpha\beta} - i_{\alpha\beta}\right) \tag{22}$$

$$J\frac{d\omega^*_m}{dt} - T^*_e\left(i^*_{\alpha\beta}, \theta_e\right) - f_{fv}\left(\omega^*_m - \omega_m\right) = 0. \tag{23}$$

Let us define the function $V^*_f(\varepsilon_i)$, which represents the reference energy given as:

$$V^*_f(\varepsilon_i) = \frac{1}{2}\varepsilon_i^T\left(L_{\alpha\beta}\varepsilon_i\right), \tag{24}$$

where $\varepsilon_i = (i^*_{\alpha\beta} - i_{\alpha\beta})$ denotes the tracking error of the current. Derivative of $V^*_f(\varepsilon_i)$ along (22), gives:

$$\dot{V}^*_f(\varepsilon_i) = -\varepsilon_i^T\left(R_{\alpha\beta}\varepsilon_i + \left(v_{\alpha\beta} - v^*_{\alpha\beta}\right)\right). \tag{25}$$

Thus, the controller law is deduced as follows:

$$v_{\alpha\beta} = v^*_{\alpha\beta} - B_i\varepsilon_i, \tag{26}$$

where $B_i = b_i I_2$ and I_2 denotes the matrix identity.

Remark 2: the term $B_i\varepsilon_i$ expressed by Eq. 26 represents the damping term which is injected to make the PMSG strictly passive, where a suitable choice of the gain b_i permits to matrix B_i to improves the tracking error convergence and addresses the parameter disturbances faced by the closed loop.

The proof of the convergence is given as follows:

Considering Eq. 25, where according to $L_{\alpha\beta}$ and the Rayleigh, it yields the inequality given as follows:

$$0 \le \lambda_{\min}\left\{L_{\alpha\beta}\right\}\|\varepsilon_i\|^2 \le V^*_f(\varepsilon_i) \le \lambda_{\max}\left\{L_{\alpha\beta}\right\}\|\varepsilon_i\|^2, \tag{27}$$

where $\lambda_{\max}\{L_{\alpha\beta}\}$ and $\lambda_{\min}\{L_{\alpha\beta}\}$ denotes maximum and minimum eigenvalues of $L_{\alpha\beta}$.

According to dissipation term $R_{\alpha\beta} + B_i$ and the Rayleigh quotient, the derivative of (28) along (26) and (27) yields the inequality given as follows:

$$\dot{V}^*_f(\varepsilon_i) = -\varepsilon_i^T\left(R_{\alpha\beta} + B_i\right)\varepsilon_i \le -\lambda_{\min}\left\{R_{\alpha\beta} + B_i\right\}\|\varepsilon_i\|^2, \ \forall t \ge 0, \tag{29}$$

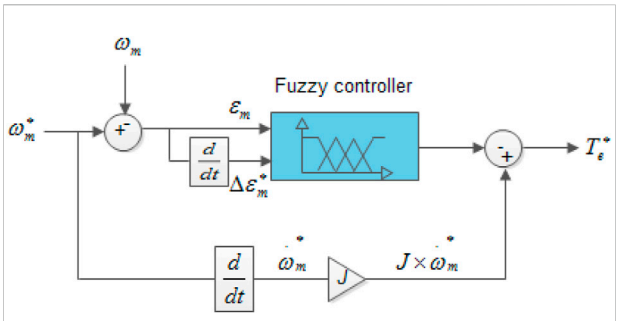

FIGURE 3
Desired torque computation.

where $\lambda_{\min}\{R_{\alpha\beta} + B_i\} > 0$ denotes minimum eigenvalue of the matrix $R_{\alpha\beta} + B_i$.

From (28) and (29), it yields:

$$\dot{V}^*_f(\varepsilon_i) = -r_1 V^*_f(\varepsilon_i), \tag{30}$$

where $r_1 = \frac{\lambda_{\min}\{R_{\alpha\beta}+B_i\}}{\lambda_{\max}\{L_{\alpha\beta}\}} > 0$.

Integrating (30), yields:

$$\dot{V}^*_f(\varepsilon_i) \le V^*_f(0)e^{-r_1 t}. \tag{31}$$

From (28) and (31), we get:

$$\|\varepsilon_i\| \le r_2\|\varepsilon_i\|e^{-r_1 t}, \tag{32}$$

where $r_2 = \sqrt{\frac{\lambda_{\min}\{L_{\alpha\beta}\}}{\lambda_{\min}\{L_{\alpha\beta}\}}} > 0$.

Thus, $\boldsymbol{\varepsilon_i}$ is exponentially decreasing with convergence of $\boldsymbol{r}_1$.

To forces the PMSG works at an optimal torque, the reference current is chosen as follows (Yang et al., 2018a):

$$i^*_{\alpha\beta} = \frac{2T^*_e}{3p\psi_f}\begin{bmatrix} -\sin(\theta_e) \\ \cos(\theta_e) \end{bmatrix}. \tag{33}$$

From Equation 23, the reference torque is formulated as follows:

$$T^*_e = J\frac{d\omega^*_m}{dt} - f_{fv}\left(\omega^*_m - \omega_m\right), \tag{34}$$

where $\varepsilon_m = (\omega^*_m - \omega_m)$ denotes the tracking error between the turbine and PMSG. The suitable dynamic is to reduce this speed tracking error as much as possible. As can be seen from the aforementioned Eq. 34, the desired torque T^*_e has two drawbacks: the dependence of its convergence on the PMSG mechanical parameters (J, f_{fv}), and it is in open-loop (Belkhier et al., 2022). To address these issues, in Belkhier et al. (2020), the term (f_{fv}) was removed, and T^*_e was computed by a PID controller. However, the authors mentioned this strategy still has a drawback with the change of J due to the fixed gains of the PID. Thus, to address this inconvenient, an FLC is introduced to replace the PID loop to solve the problem caused by imprecise

TABLE 1 Fuzzy logic rules.

$\Delta\varepsilon_m$ / ε_m	NB	NS	Z	PS	PB
NB	NB	NB	NS	NS	Z
NS	NB	NB	NS	Z	PS
Z	NS	NS	Z	PS	PS
PS	NS	Z	PS	PB	PB
PB	Z	PS	PS	PB	PB

parameters, to guarantee convergence of ε_m, eliminates the static error, and ensures robustness. The design process of T_e^* is depicted by Figure 3.

The fuzzy manager is used for gain adjustment, which satisfies the requirements induced by inaccurate variables. The fuzzy values are either the speed error ε_m in the instance of the regulator equation calculation in (34) or its derivation. Fuzzy controller rules are exposed in Table 1, which are defined as: zero (Z), negative small (NS), positive small (PS), positive big (PB), positive medium (PM), negative medium (NM), and negative big (NB). To choose the membership functions shown in Figure 4, symmetrical and equally distributed triangular and trapezoidal types are utilized. The mechanism for splitting these functions is provided according to Lee and Takagi (Michael and Takagi, 1993) and Yubazaki et al. (1995). Their approach is predicated on the notion that many membership functions might share a single parameter. The benefit of this approach is that it significantly reduces the number of parameters required by the membership functions. The center of gravity defuzzication approach is used to generate the crisp outputs, and a max–min fuzzy inference is used to produce the decision-making output.

Grid-side model and PI controller

The GSC is modelized as given in Figure 5. The classical PI method is selected to regulate the GSC, which is formulated as (Yang et al., 2018a; Belkhier et al., 2020):

$$\begin{bmatrix} V_d \\ V_q \end{bmatrix} = R_f \begin{bmatrix} i_{df} \\ i_{qf} \end{bmatrix} + \begin{bmatrix} L_f \dfrac{di_{df}}{dt} - \omega L_f i_{qf} \\ L_f \dfrac{di_{qf}}{dt} + \omega L_f i_{df} \end{bmatrix} + \begin{bmatrix} V_{gd} \\ V_{gq} \end{bmatrix}, \quad (35)$$

where ω indicates the angular frequency, V_{gd} and V_{gq} are the grid voltages, i_{df} and i_{qf} indicate the currents, L_f indicates the inductance, V_d and V_q indicate inverter voltages, and R_f indicates resistance of the filter. The mathematical formalism

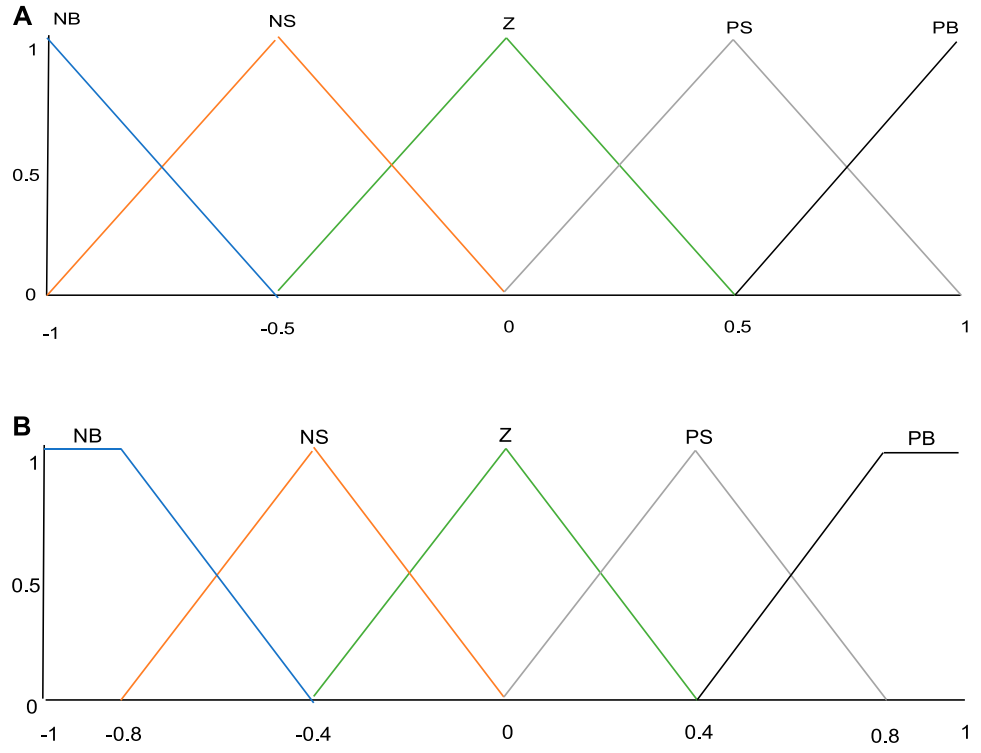

FIGURE 4
Fuzzy rules. **(A)** Function's inputs **(B)** Outputs function.

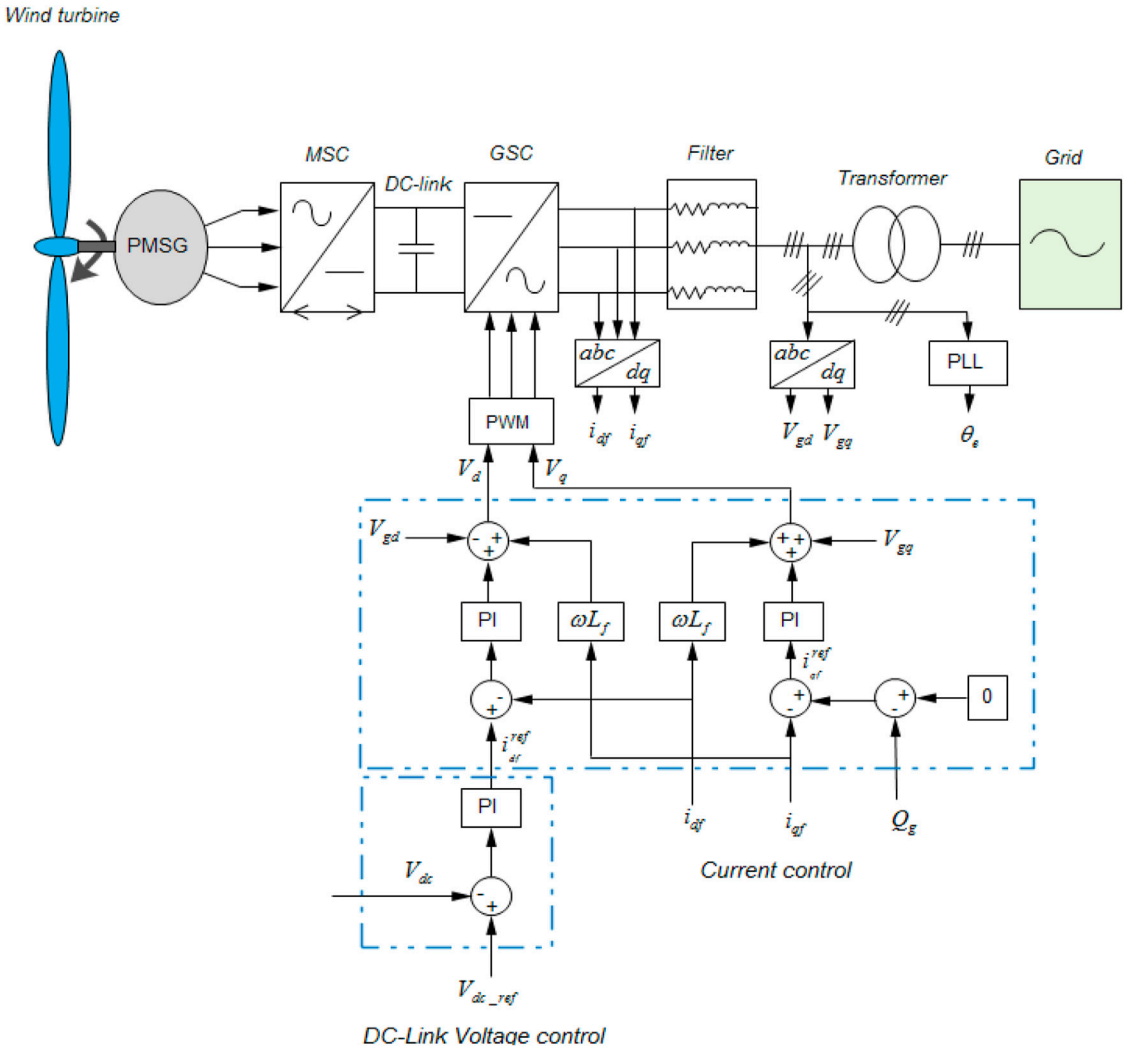

FIGURE 5
GSC PI controller schematic.

for the converter link voltage is given by (Subramaniam and Joo, 2019):

$$C\frac{dV_{dc}}{dt} = \frac{3}{2}\frac{v_{gd}}{V_{dc}}i_{df} + i_{dc}, \tag{36}$$

where C is the DC-link capacitance, i_{dc} is the line current, and V_{dc} is the DC-link voltage. The PI loop designs are as follows:

$$\begin{cases} V_{gd}^{PI} = k_{gp}^{d}\left(i_{df}^{ref} - i_{df}\right) - k_{gi}^{d}\int_0^t \left(i_{df}^{ref} - i_{df}\right)d\tau \\ V_{gq}^{PI} = k_{gp}^{q}\left(i_{qf}^{ref} - i_{qf}\right) - k_{gi}^{q}\int_0^t \left(i_{qf}^{ref} - i_{qf}\right)d\tau \end{cases}, \tag{37}$$

$$i_{qf}^{ref} = k_{dcp}\left(V_{dc\_ref} - V_{dc}\right) - k_{dci}\int_0^t \left(V_{dc\_ref} - V_{dc}\right)d\tau, \tag{38}$$

where $k_{gp}^{d} > 0$, $k_{gi}^{d} > 0$, $k_{gp}^{q} > 0$, $k_{gi}^{q} > 0$, $k_{dcp} > 0$, and $k_{dci} > 0$. The active and reactive powers are given as:

$$\begin{cases} P_g = \frac{3}{2}V_{gd}i_{df} \\ Q_g = \frac{3}{2}V_{gd}i_{qf} \end{cases}. \tag{39}$$

Extensive numerical investigation and experimental validation

For the simulation of the system, the average value of the wind speed is fixed at 12 m/s, and the reference of the wind

TABLE 2 Parameters of the system.

Parameter	Value
Air density (ρ)	1.24 kg/m^2
Stator resistance (R_s)	0.006 Ω
Turbine radius (R)	33.5 m
Stator inductance (L_{dq})	0.3 mH
Pole pairs number (p)	48
Flux linkage (ψ_f)	1.48 Wb
Total inertia (J)	35,000 kg m^2
DC-link capacitor (C)	2.9 F
Grid voltage (V_g)	574 V
DC-link voltage (V_{dc})	1150 V
Grid-filter resistance (R_f)	0.3 pu
Grid-filter inductance (L_f)	0.3 pu

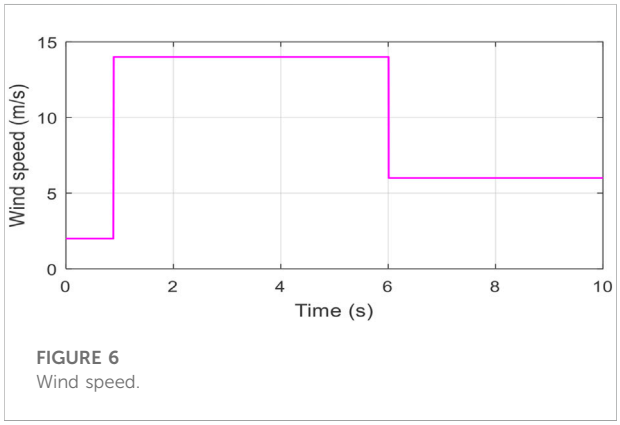

FIGURE 6
Wind speed.

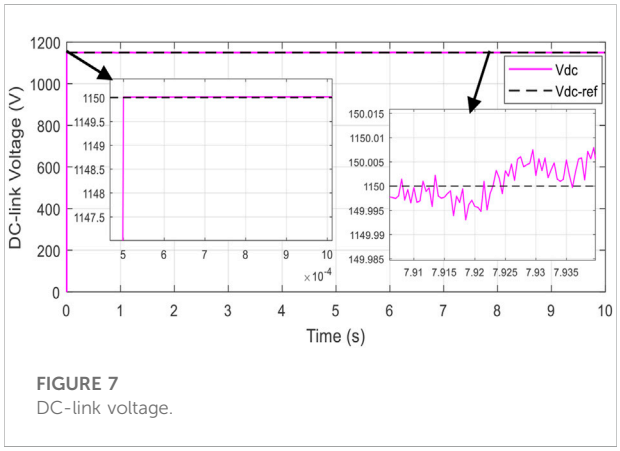

FIGURE 7
DC-link voltage.

turbine speed ref is estimated from the generator. The reference of the reactive power is set to 0 kVAr. The parameter values of the system are given in Table 2. The reference of the DC-bus voltage is set to 1150 V. The network is assumed to have infinite power, which allows the injection of all the production without

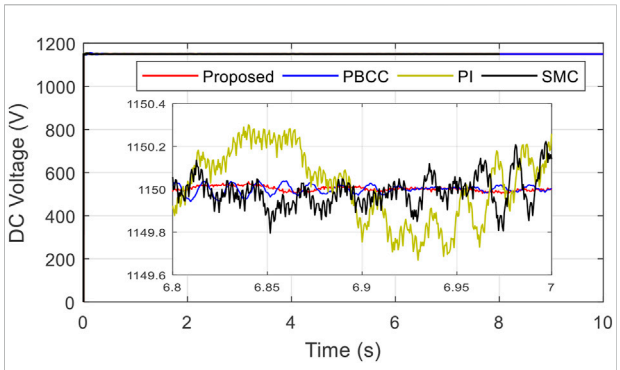

FIGURE 8
DC-link response compared with conventional controls.

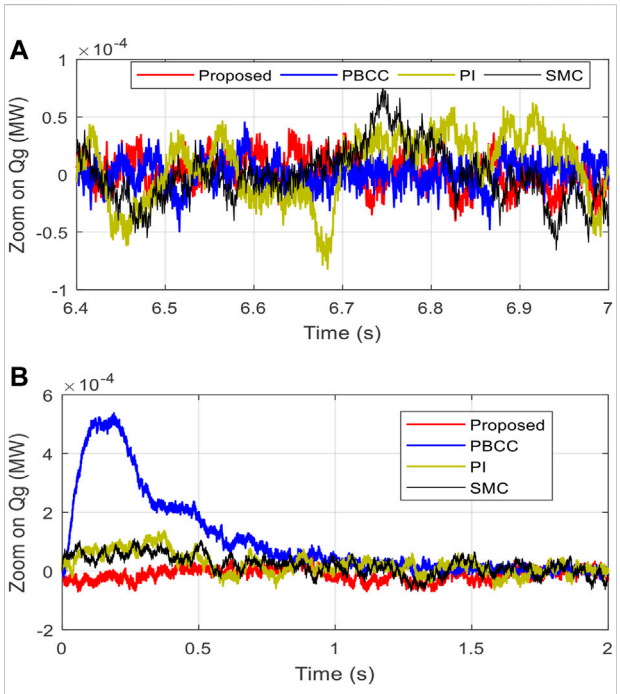

FIGURE 9
Reactive power response of the tested controls.

constraints. The damping value is $b_i = 250$. The fixed gains are $k_{dcp} = 5$, $k_{dci} = 500$, $k^d_{gp} = k^q_{gp} = 9$, and $k^d_{gi} = k^q_{gi} = 200$. For a better analysis of the performance of the adopted strategy, a comparison with other techniques was illustrated, with the conventional (PI) method, passivity-based current control (PBCC) proposed in Belkhier et al. (2020), and the SMC. The suggested approach is put to the test in two situations: First, the suggested regulator is evaluated using the PMSG's starting settings and evaluated to the standard controllers. The next aim is to analyze the resilience of this suggested fuzzy-EBC in the face of fluctuation. Finally,

TABLE 3 Results comparison of the control strategies.

Control	Proposed		PBCC		PI		SMC	
Variation	R_s, J	2 R_s 2J	R_s, J	2 R_s 2J	R_s, J	2 R_s 2J	R_s, J	2 R_s 2J
ε (V_{dc})	±0.005	±0.005	±0.02	±0.04	±0.2	±0.4	±0.2	±0.3
ε (Q_g)	±4e-5	±4e-5	±5e-5	±5.5e-5	±8e-5	±9e-5	±7e-5	±8e-5
Convergence speed (V_{dc})	0.6 s	0.6 s	1 s	1.2 s	1.4 s	1.8 s	1.6 s	1.8 s
Convergence speed (Q_g)	0.6 s	0.6 s	0.6 s	0.8 s	1 s	1.2 s	0.55 s	0.8 s

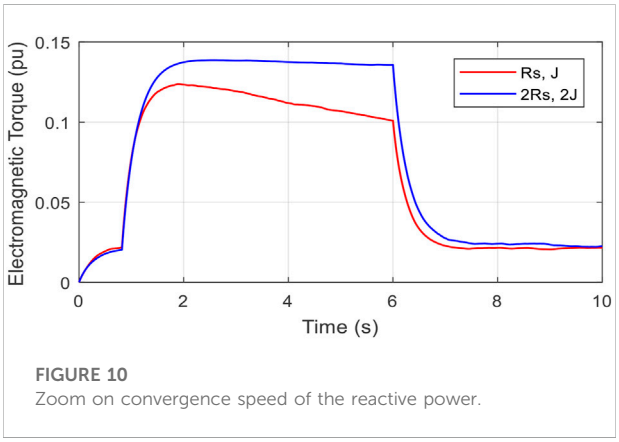

FIGURE 10
Zoom on convergence speed of the reactive power.

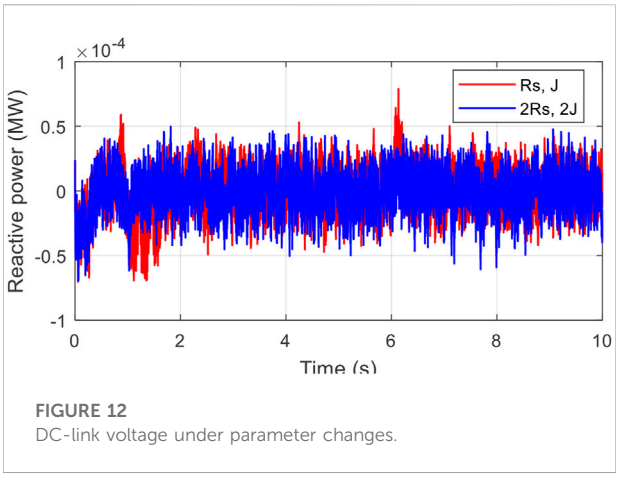

FIGURE 12
DC-link voltage under parameter changes.

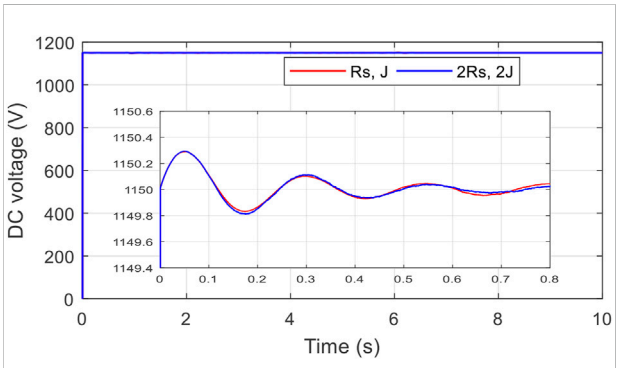

FIGURE 11
Electromagnetic torque under parameter changes.

experimental analysis utilizing PIL testing is performed to establish the practicality of the proposed system.

Fixed parameters performance analysis

Figure 6 indicates the wind velocity profile applied on the conversion mechanism. Figure 7 depicts the DC-bus trailing behavior with exceptionally low error (ε (V_{dc})). The suggested method produces transitory deflates of -0.005 and messes up of +0.005. The DC power reaction owing to suggested fuzzy-PBC, SMC, PBCC, and PI benchmarks is indicated in Figure 8. Transient undershoots of -0.02, -0.2, and -0.2 are recorded with the PBCC, PI, and SMC techniques, respectively, and transient messes up of +0.02, +0.2, and +0.2 are noted with the PBCC, PI, and SMC methodologies, respectively.

Figure 9 depicts the tracking error (ε (Q_g)) caused by the examined fuzzy-EBC, PBCC, PI, and SMC, with intermittent underneath and messes up of -4e-5, -5e-5, -8e-5, -7e-5, and +4e-5, +5e-5, +8e-5, +7e-5, correspondingly. Therefore, the recommended methodology, as shown in Table 3, has the smallest underneath and overreach. Furthermore, the suggested approach (0.3s) outperforms the PBCC (1s), PI (0.6s), and SMC (0.55s) in terms of relatively stable inaccuracy and converging ratio, as demonstrated in Figure 9; Table 3. It is deduced that the suggested PBC guaranteed faster response time, greater productivity, and lower following faults as compared to the standard nonlinear techniques studied.

Parameter changes performance analysis

In the present sub-section, simultaneous changes of +100% R_s and J are applied on the PMSG model to illustrate the robustness properties of the present method. Figure 10 indicates T_e behavior under fixed and varied conditions. It is

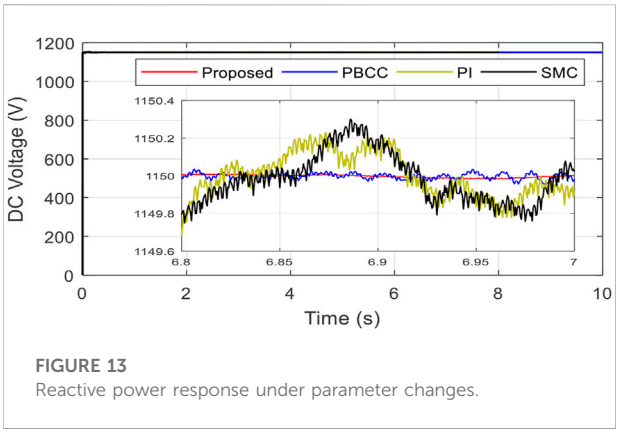

FIGURE 13
Reactive power response under parameter changes.

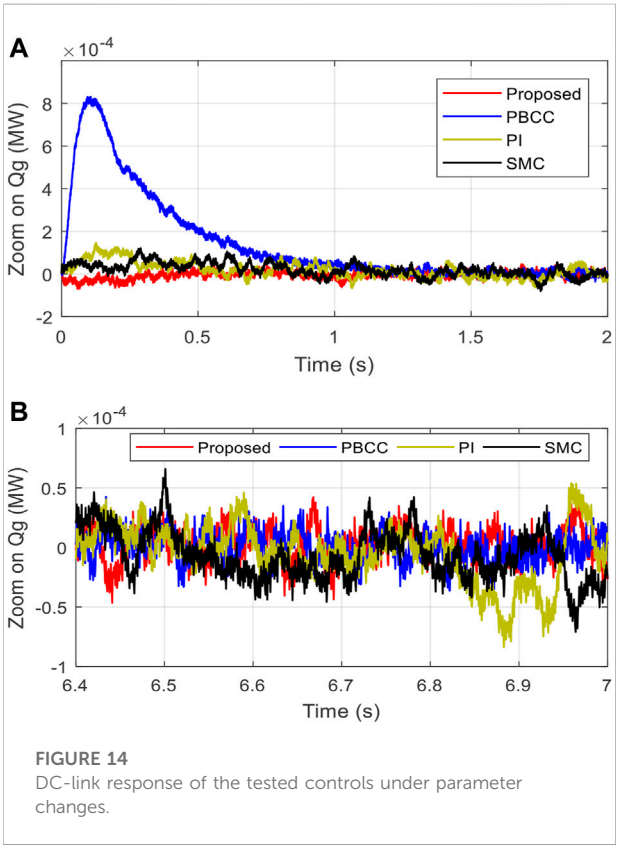

FIGURE 14
DC-link response of the tested controls under parameter changes.

evident that at t = 1–8s, the investigated fuzzy-EBC generate a higher torque with a constant steady-state under variation conditions (0.14 pu) than the one generated under initial parameter conditions (0.12 pu), an increase on the generated T_e of 16.53%. Figure 11 depicts V_{dc} answer caused by the suggested alternative within every scenario, in which error ε (V_{dc}) answer and monitoring inaccuracy equal to 0 are almost observed, that is, 0.05 as per Table 3.

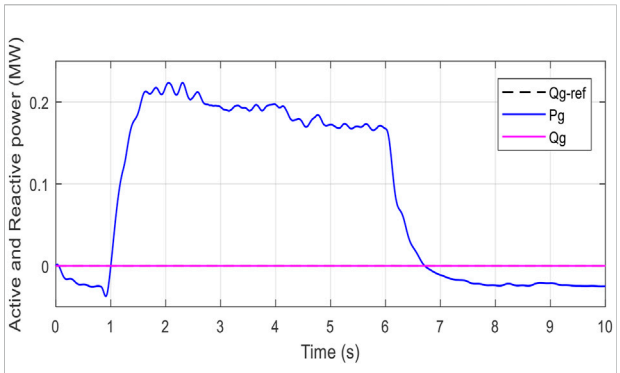

FIGURE 15
Reactive power response of the tested controls under parameter changes.

Figure 12 indicates the resemblance monitoring reaction of Q_g to R_s and J perturbations. According to the findings, the suggested fuzzy-EBC demonstrates the same Q g behavior including both variable and fixed attribute values, where the recorded Q_g error ε (Q_g) is approximately the same as in case 1, that is, ±4.5e-5. The measured values of both V_{dc} and Q_g are tabulated in Table. 3.

Figure 13 depicts the V_{dc} response for all the PBCC, PI, SMC, and proposed fuzzy-PBC. As indicated in Table 3, the PBCC has a path loss of ±0.04, the PI has a path loss of ±0.4, and the SMC has a path loss of ±0.3. As shown in Table 3, the suggested technique obviously provides a constant V_{dc} error and greater trajectory tracking rate when opposed to the other competitors, that are either susceptible to combined perturbations of R_s and J. The Q g answer for all of the investigated controllers is indicated in Figure 14.

As per the reported findings, the suggested fuzzy-EBC has a lower tracking error below these variations than PBCC (5.5e-5), PI (9e-5), and SMC (8e-5), as shown in Table 3. Moreover, the suggested fuzzy-PBC clearly outperforms the other alternatives in terms of velocity position error ε (Q_g) although when exposed to simultaneous perturbations, as demonstrated in Figure 14 and Table 3. Hence, based on the actual analysis and Table 4, the suggested alternative outperforms the other comparable methodologies of resilience, quick reaction and rapid converging, and effectiveness. This verified the theoretical findings of *parameter changes performance analysis*. Furthermore, as shown in Figures 15–17, the closed loop operates at full power and integrates an effective electricity to the network.

Experimental testing

The processor-in-the-loop testing (PiL) is the process of testing and validating embedded software on the processor before it is utilized in the electronic control unit (ECU). Algorithms and functions are often created on a PC in a development environment. More details about processor-in-

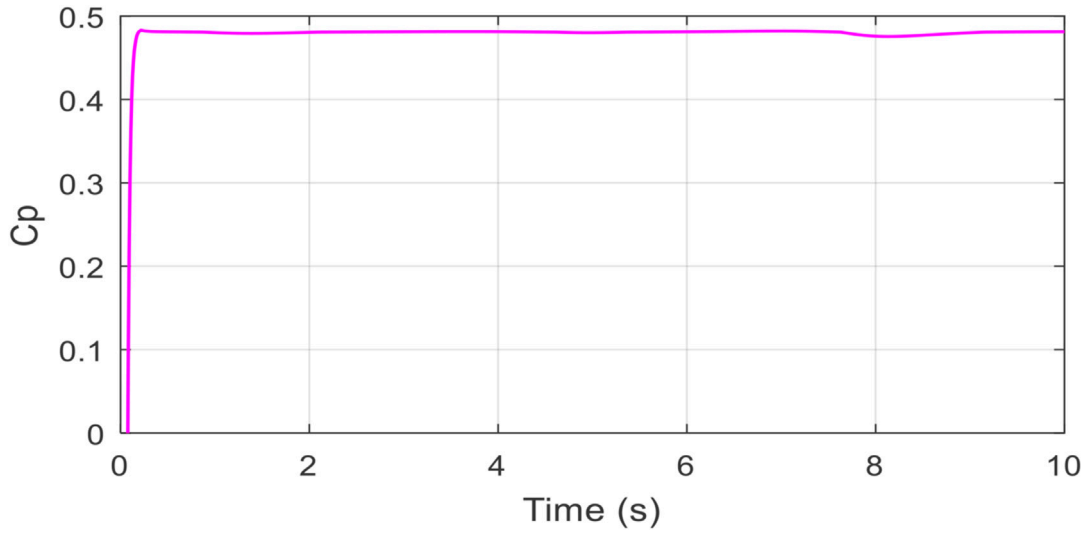

FIGURE 16
Zoom on reactive power response of the tested controls under parameter changes

TABLE 4 Performance comparisons of the tested controls.

Controls	Proposed	PBCC	SMC	PI
Response speed	Extremely fast (0.8e-3 s)	Very fast (1e-3 s)	Fast (1.2e-3 s)	Slow (2e-3 s)
Stability	Highly stable (fluctuations free)	Very stable (fluctuations free)	Stable (with fluctuations)	Poor stability (with fluctuations)
Robustness	High robustness	Robust	Not robust	Not robust
Performance	Higher	Good	Low	Low

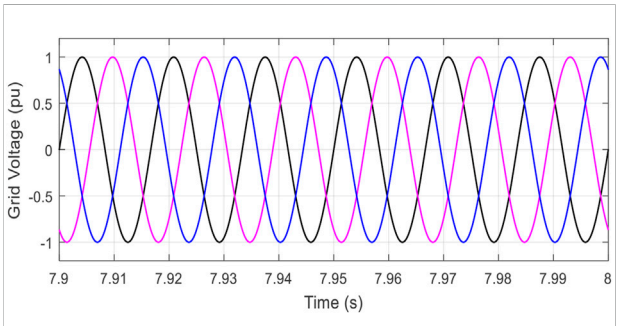

FIGURE 17
Active and reactive powers response.

the loop experimentation are reported in Ullah et al. (2020); Ullah et al. (2021a); Ullah et al. (2021b). PiL tests are run to ensure that the built code also runs on the target CPU. The control algorithms for the PiL test are often run on a device known as an evaluation board. PiL testing is sometimes run on the actual ECU. Both types use the controller's actual processor rather than the PC as in software-in-loop (SiL) testing. The target processor offers the advantage of detecting compiler issues. As a result of the preceding work, the suggested control systems are evaluated utilizing PIL investigation, and the block diagram of the setup is illustrated in Figure 18. In the PIL investigation, the DSP command board is physically interconnected with the simulated converter system. The control board is made up of a double core processor TMS320F379D that was developed using the Simulink planet's simple synthesis approach. Simulink is used to create discontinuous versions of the described devices, and the output or hex file is loaded into the processor's random-access memory (RAM).

In PiL testing, "in-the-loop" indicates that the controller is integrated in physical machine and the program during test's surroundings is emulated. The wind profile utilized in the PIL testing is depicted in Figure 19. Figures 20 and 21, which demonstrate the experimental findings for DC-link voltage, active, and reactive powers obtained using the PIL approach.

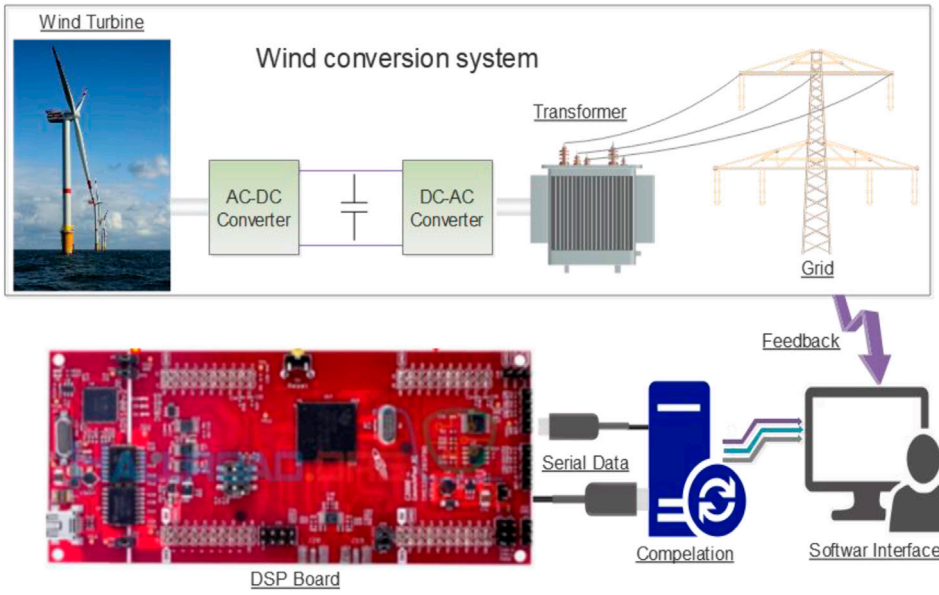

FIGURE 18
Experimental Step.

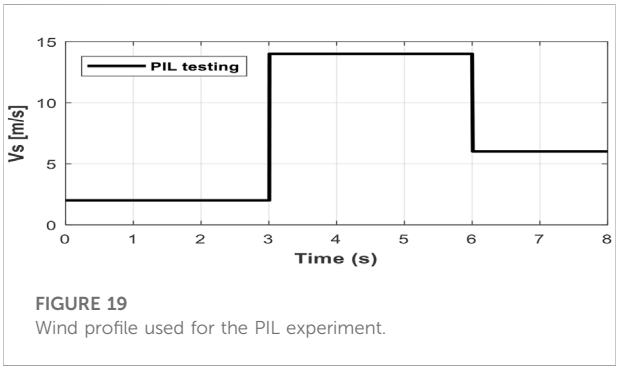

FIGURE 19
Wind profile used for the PIL experiment.

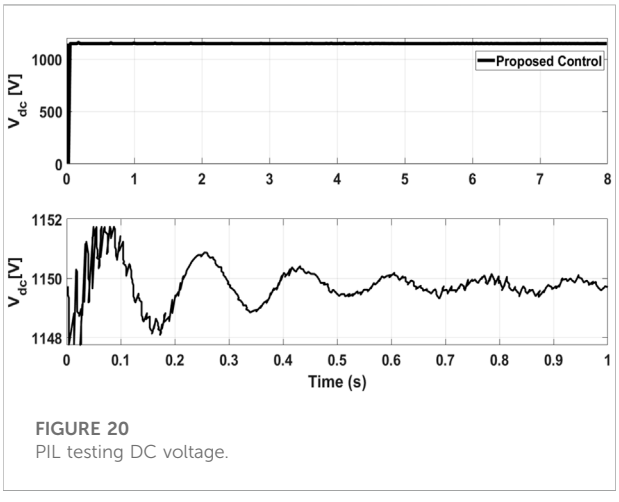

FIGURE 20
PIL testing DC voltage.

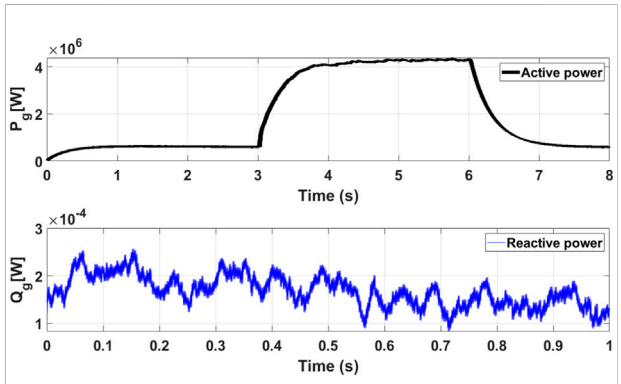

FIGURE 21
PIL testing grid powers.

Based on the provided data, the proposed fuzzy-EBC is definitely applicable in practice.

6 Conclusion

For a PMSG in a wind power converter, a new fuzzy energy-based controller is presented. To obtain the maximum power out of wind energy, utilize the suggested strategy where the entire dynamics of the PMSG is considered when designing the control law. A fuzzy controller is selected to guarantee the overall-rated speed operation of the PMSG, and then compute a higher reference torque. Dynamic

simulations of the studied system under parameter changes have taken special attention, and the results have been compared to conventional methods, which show a quick track of the DC voltage and reactive energy to their set values over the compared controls. All of the conversion system's flaws have been fixed, and the goals have been met. The designed control approach offers optimum performance as well as increased resilience. Moreover, the PIL experiment is conducted to prove that the proposed controller is practically implementable. Future works will be focused on:

- Experimental validation of the proposed control on a real wind energy system.
- The adaptation of the damping fixed gain by introducing an optimization algorithm.

Data availability statement

The original contributions presented in the study are included in the article/Supplementary Material; further inquiries can be directed to the corresponding author.

Author contributions

All authors listed have made a substantial, direct, and intellectual contribution to the work and approved it for publication.

Conflict of interest

The authors declare that the research was conducted in the absence of any commercial or financial relationships that could be construed as a potential conflict of interest.

Publisher's note

All claims expressed in this article are solely those of the authors and do not necessarily represent those of their affiliated organizations, or those of the publisher, the editors, and the reviewers. Any product that may be evaluated in this article, or claim that may be made by its manufacturer, is not guaranteed or endorsed by the publisher.

References

Belkhier, Y., and Achour, A. (2020). Fuzzy passivity-based linear feedback current controller approach for PMSG-based tidal turbine. *Ocean. Eng.* 218, 108156. doi:10.1016/j.oceaneng.2020.108156

Belkhier, Y., Achour, A., Ullah, N., Shaw, R. N., Chowdhury, S., and Techato, K. (2022). Energy-based fuzzy supervisory non integer control for performance improvement of PMSG-Based marine energy system under swell effect and parameter uncertainties. *Renew. Energy* 186, 457–468. doi:10.1016/j.renene.2021.12.126

Belkhier, Y., and Achour, A. Y. (2020). An intelligent passivity-based backstepping approach for optimal control for grid-connecting permanent magnet synchronous generator-based tidal conversion system. *Int. J. Energy Res.* 45, 5433–5448. doi:10.1002/er.6171

Belkhier, Y., Achour, A. Y., Ullah, N., and Shaw, R. N. (2020). Modified passivity-based current controller design of permanent magnet synchronous generator for wind conversion system. *Int. J. Model. Simul.* 42, 192–202. doi:10.1080/02286203.2020.1858226

Bigarelli, L., Benedetto, M. D., Lidozzi, A., Solero, L., Odhano, S. A., and Zanchetta, P. (2020). PWM-based optimal model predictive control for variable speed generating units. *IEEE Trans. Ind. Appl.* 56 (1), 541–550. doi:10.1109/tia.2019.2955662

Chandrasekaran, K., Mohanty, M., Golla, M., Venkadesan, A., and Simon, S. P. (2020). Dynamic MPPT controller using cascade neural network for a wind power conversion system with energy management. *IETE J. Res.*, 1–15. doi:10.1080/03772063.2020.1756934

Soliman, M. S., Belkhier, Y., Ullah, N., Achour, A., Alharbi, Y. M., Al Alahmadi, A. A., et al. (2021). Supervisory energy management of a hybrid battery/PV/tidal/wind sources integrated in DC-microgrid energy storage system. *Energy Reports* 7, 7728–7728.

Fantino, R., Solsona, J., and Busada, C. (2016). Nonlinear observer-based control for PMSG wind turbine. *Energy* 113, 248–257. doi:10.1016/j.energy.2016.07.039

Haq, I. U., Khan, Q., Khan, I., Akmeliawati, R., and Nisar, K. S. (2020). Maximum power extraction strategy for variable speed wind turbine system via neuro-adaptive generalized global sliding mode controller. *IEEE Access* 8, 128536–128547. doi:10.1109/access.2020.2966053

Jlassi, I., and Cardoso, A. J. M. (2019). Fault-tolerant back-to-back converter for direct-drive PMSG wind turbines using direct torque and power control techniques. *IEEE Trans. Power Electron.* 34 (11), 11215–11227. doi:10.1109/tpel.2019.2897541

Michael, A., and Takagi, H. (1993). "Dynamic control of genetic algorithms using fuzzy logic techniques," in Proceedings of the Fifth International Conference on Genetic Algorithms (Morgan Kaufmann), 76–83.

Mohammadi, E., Fadaeinedjad, R., and Nadji, H. R. (2019). Design, electromechanical simulation, and control of a variable speed stall-regulated PMSG-based wind turbine. *Int. J. Green Energy* 16 (12), 890–900. doi:10.1080/15435075.2019.1641714

Nicklasson, P. J., Ortega, R., and Espinosa-Perez, G. (1994). Passivity-based control of the general rotating electrical machine. *Proc. 1994 33rd IEEE Conf. Decis. Control* 4, 4018–4023. doi:10.1109/CDC.1994.411573

Rizk-Allah, R. M., Hassanien, A. E., and Song, D. (2022). Chaos-opposition-enhanced slime mould algorithm for minimizing the cost of energy for the wind turbines on high-altitude sites. *ISA Trans.* 121, 191–205. doi:10.1016/j.isatra.2021.04.011

Saidi, Y., Mezouar, A., Miloud, Y., Kerrouche, K. D. E., Brahmi, B., and Benmahdjoub, M. A. (2019). Advanced non-linear backstepping control design for variable speed wind turbine power maximization based on tip-speed-ratio approach during partial load operation. *Int. J. Dyn. Control* 8, 615–628. doi:10.1007/s40435-019-00564-3

Song, D., Li, Z., Wang, L., Jin, F., Huang, C., Xia, E., et al. (2022). Energy capture efficiency enhancement of wind turbines via stochastic model predictive yaw control based on intelligent scenarios generation. *Appl. Energy* 312, 118773. doi:10.1016/j.apenergy.2022.118773

Song, D., Tu, Y., Wang, L., Jin, F., Li, Z., Huang, C., et al. (2022). Coordinated optimization on energy capture and torque fluctuation of wind turbines via variable weight NMPC with fuzzy regulator. *Appl. Energy* 312, 118821. doi:10.1016/j.apenergy.2022.118821

Subramaniam, R., and Joo, Y. H. (2019). Passivity-based fuzzy ISMC for wind energy conversion systems with PMSG. *IEEE Trans. Syst. Man. Cybern. Syst.* 51, 2212–2220. doi:10.1109/tsmc.2019.2930743

Ullah, N., Farooq, Z., Sami, I., Chowdhury, M. S., Techato, K., and Alkhammash, H. I. (2020). Industrial grade Adaptive control scheme for a micro-grid integrated dual active bridge driven battery storage system. *IEEE Access* 8, 210435–210451. doi:10.1109/ACCESS.2020.3039947

Ullah, N., Sami, I., Chowdhury, M. S., Techato, K., and Alkhammash, H. I. (2021a). Artificial intelligence integrated fractional order control of doubly fed induction generator-based wind energy system. *IEEE Access* 9, 5734–5748. doi:10.1109/ACCESS.2020.3048420

Ullah, N., Sami, I., Jamal Babqi, A., I Alkhammash, H., Belkhier, Y., Althobaiti, A., et al. (2021b). Processor in the loop verification of fault tolerant control for a three phase inverter in grid connected PV system. *Energy Sources, Part A Recovery, Util. Environ. Eff.*, 1–17. doi:10.1080/15567036.2021.2015486

Wang, X., and Wang, S. (2020). Adaptive fuzzy robust control of PMSM with smooth inverse based dead-zone compensation. *Int. J. Control Autom. Syst.* 14 (2), 378–388. doi:10.1007/s12555-015-0010-6

Yang, B., Wu, Q. H., Tiang, L., and Smith, J. S. (2013). *Adaptive passivity-based control of a TCSC for the power system damping improvement of a PMSG based offshore wind farm*. Madrid, Spain: IEEE International Conference on Renewable Energy Research and Applications ICRERA, 1–5.

Yang, B., Yu, H., Zhang, Y., Chen, J., Sang, Y., Jing, L., et al. (2018a). Passivity-based sliding-mode control design for optimal power extraction of a PMSG based variable speed wind turbine. *Renew. Energy* 119, 577–589. doi:10.1016/j.renene.2017.12.047

Yang, B., Yu, T., Shu, H., Qiu, D., Zhang, Y., Cao, P., et al. (2018b). Passivity-based linear feedback control of permanent magnetic synchronous generator-based wind energy conversion system: Design and analysis. *IET Renew. Power Gener.* 12 (9), 981–991. doi:10.1049/iet-rpg.2017.0680

Yubazaki, N., Otani, M., Ashida, T., and Hirota, K. (1995). "Dynamic fuzzy control method and its application to positioning of induction motor," in Proceedings of 1995 IEEE International Conference on Fuzzy Systems (IEEE), 1095–1102.3

Zargham, F., and Mazinan, A. H. (2019). Super-twisting sliding mode control approach with its application to wind turbine systems. *Energy Syst.* 10, 211–229. doi:10.1007/s12667-018-0270-3